

The rise of FTIR spectroscopy in the characterization of asymmetric lipid membranes

Lea Pašalić^{a, †}, Petra Maleš^{a, †}, Ana Čikoš^b, Barbara Pem^a, Danijela Bakarić^{a, *}

^a Division for Organic Chemistry and Biochemistry, Ruđer Bošković Institute, Bijenička 54, 10000 Zagreb, Croatia

^b The Centre for Nuclear Magnetic Resonance (NMR), Ruđer Bošković Institute, Bijenička 54, 10000 Zagreb, Croatia

*Corresponding author. E-mail: danijela.bakaric@irb.hr (Danijela Bakarić)

† (L. P., P. M.) Both authors contributed equally to the manuscript.

Abstract

In contrast to symmetric unilamellar liposomes (sLUVs) prepared from a mixture of different lipids, asymmetric ones (aLUVs) with different lipid composition in the inner and outer membrane leaflets are more suitable model systems of eukaryotic plasma membranes. However, apart from the challenging preparation of asymmetric liposomes and small amounts of obtained asymmetric unilamellar liposomes (aLUVs), a major drawback is the qualitative characterization of asymmetry, as each of the techniques used so far has certain limitations. In this regard, we prepared aLUVs composed dominantly of DPPC(out)/DPPS(in) lipids and, along with ¹H NMR and DSC characterization, we showed for the first time how FTIR spectroscopy can be used in the presence of (a)symmetry between DPPC/DPPS lipid bilayers. Using second derivative FTIR spectra we demonstrated not only that the hydration of lipids glycerol backbone and choline moiety of DPPC differs in s/aLUVs, but in addition that the lateral interactions between hydrocarbon chains during the phase change display different trend in s/aLUVs. Molecular dynamics simulations confirmed different chain ordering and packing between s/a bilayers, with a significant influence of temperature, i.e. membrane phase.

Keywords: 1,2-dipalmitoyl-*sn*-glycero-3-phosphocholine (DPPC); 1,2-dipalmitoyl-*sn*-glycero-3-phosphoserine (DPPS); asymmetric large unilamellar liposomes (LUVs); ¹H NMR and FTIR spectroscopy, differential scanning calorimetry (DSC); molecular dynamics (MD) simulations

1. Introduction

Plasma membranes (PMs) are predominantly lipid- and protein-based assemblies organized as bilayers that are responsible for controlling the exchange of substances between the cytosol and the extracellular space. Although they were initially considered to be mere physical barriers that compartmentalize cellular material and an inert matrix for immersion of integral proteins, nowadays it is recognized that the elasticity of the PMs lipid scaffold actively contributes to the transport of matter by *exo*- and *endo*cytosis, as well as the production of extracellular vesicles [1–3]. The ability of the lipid bilayer to change the shape in response to a physical or (bio)chemical stimulus [4] is a consequence of the inhomogeneous distribution of different lipids not only in individual but also in opposing membrane leaflets, which inevitably leads to the asymmetry of PMs. The most prominent features of PM asymmetry are reflected in the different composition of extracellular and cytosolic lipids; specifically, the outer leaflet is rich in sphingomyelin (SM) which, together with cholesterol and glycosphosphatidylinositol (GPI)-anchored proteins [5] forms lipid rafts (LRs), small (10-200 nm) and highly dynamic domains thought to be responsible for membrane trafficking and signal transduction [6] that are located in the extracellular leaflet. The opposite cytosolic leaflet contains almost exclusively phosphatidylethanolamines (PEs), zwitterionic lipids that favor negatively curved surfaces due to their intrinsic conical shape [7], and phosphatidylserines (PSs), anionic lipids that signal the loss of PM integrity and cell apoptosis [8] when translocated into the extracellular leaflet.

In order to understand certain structural and dynamic features of PM, one mainly resorts to the research of model lipid membranes, where the effects of interest can be manifested in a targeted manner, and the phenomena that interfere with them can be suppressed or eliminated. Numerous experimental and computational studies that have been carried out over the years on model lipid membranes have provided an approximate insight into processes such as water or ion permeation across the membrane [9,10], membrane fusion [11] and adsorption followed by the passage of cell penetrating peptides (CPPs) through the membrane [12–14]. However, many of these findings

reveal only a part of the whole mosaic because most of the researched model membranes suffer from a lack of asymmetry in the lipid composition between the inner and outer leaflet.

The key advantage of using symmetric (sLUVs) over asymmetric large unilamellar liposomes (aLUVs) as a model membrane system is their incomparably simpler preparation, stability and reproducibility. In recent years, this trend has begun to change, and several experimental protocols for the preparation of aLUVs are now being followed and continuously improved, each with its own limitations and advantages [15,16]. For example, sufficiently stable aLUVs with PS lipids in the inner leaflet can be obtained from PS-based sLUVs, in which suspension water-soluble PS decarboxylase from *Plasmodium knowlesi* was added [17]. Despite the relative simplicity of the protocol, along with the stability and sustainability of the asymmetry of the obtained liposomes, the fundamental shortcoming of the aforementioned approach is the enzymatic transformation of the PS lipids of the outer leaflet into PE lipids only and exclusively, resulting in PE(out)/PS(in) liposomes, which are not the most accurate model of PMs where PE lipids are, along with PS, predominantly found in the inner (cytosolic) leaflet [15,16]. Furthermore, the external addition of CaCl₂ salt into a suspension containing symmetric liposomes constituted from 1,2-dipalmitoyl-*sn*-glycero-3-phosphocholine (DPPC) and 1-palmitoyl-2-oleoyl-*sn*-glycero-3-phospho-L-serine (POPS) lipids leads to the formation of Ca²⁺···POPS···POPS complex that, favorizing the negative curvature, ultimately transfers to the inner liposome leaflet [18]. In contrast to the aforementioned approaches, which require either precisely defined lipid due to an enzymatic reaction (PS exclusively), or an anionic lipid due to complexation with Ca²⁺ (PS among else), there is the less invasive cyclodextrin-catalyzed exchange of outer leaflets lipids of acceptor sLUV by those in multilamellar (MLV) donor liposomes [19]. Although the popularity of this approach stems from the unlimited type of lipids that can be obtained in the outer/inner leaflet [20], the main disadvantages are relatively low yields compared to the initial amounts of lipids, rather small amounts of obtained aLUVs suspensions and ultimately high possibility from contamination of aLUVs suspension with cyclodextrin [15,16].

In the qualitative and quantitative analyses of aLUVs numerous experimental techniques are intensively used and continue to be developed to accurately determine the lipid composition of the inner and outer leaflet, and each of them is inherently superior than others in certain aspects, while being deficient in others [15,16]. Specifically, structural analysis techniques such as SAXS and

SANS provide the individual area per lipid and the thickness of the outer/inner leaflet [21], while being quite expensive and requiring high sample amounts; surface zeta-potential measurements can easily distinguish the s/aLUVs with minimal s/aLUV concentration, but the utility of anionic lipids is indispensable [17]; fluorescence spectroscopy findings are based on a different response of fluorescently-tagged lipids when located in the outer/inner leaflet [22–24] but, at the same time, may alter aLUVs surface and give a misleading picture of processes like lipid flip-flop [25,26]; calorimetric (DSC) measurements in a relatively simple fashion discriminate melting profiles for sLUVs and aLUVs due to different sizes of cooperativity units [27], lacking any other molecular-level information; ^1H NMR provides an insight into distribution of lipids between opposing leaflets in the presence of externally added Pr^{3+} that, notably, influences only choline moiety protons ($-\text{N}(\text{CH}_3)_3^+$) and is, therefore, limited to PC and SM lipids only; finally, variants of chromatographic techniques, especially those coupled with MS, allow the quantification of certain lipids in a sample fraction, but, due to the intrinsic destructivity, lipid distribution across opposing leaflets cannot be reconstructed from the results of these techniques [28,29].

To the best of our knowledge, there are no records on the applicability of FTIR spectroscopy in the identification and characterization of aLUVs so far. Since this probe-free spectroscopic technique literally captures the signatures of almost all molecules (except of homomolecular diatomic molecules), its potential remains completely unused. To demonstrate the possibilities of FTIR spectroscopy in characterizing aLUVs and distinguishing them from sLUVs in a qualitative manner, we prepared s/aLUV from DPPC and 1,2-dipalmitoyl-*sn*-glycero-3-phosphoserine (DPPS) lipids (Fig. 1) in deuterated Tris buffer (dTris) following cyclodextrin-catalyzed exchange approach [23]. The presence of aLUVs whose outer leaflet is predominantly composed of DPPC was unambiguously confirmed by ^1H NMR spectroscopy, while their melting profiles displayed qualitative differences in comparison to those of sLUVs. FTIR spectra enabled unravelling crucial distinctions in s/aLUVs features addressed to the lipid glycerol backbone and phosphate and choline moieties, which was further supported by MD simulations. More importantly, the results presented here demonstrated the supremacy of FTIR spectroscopy over ^1H NMR not only in detecting lipid signals but also in distinguishing sLUVs from aLUVs.

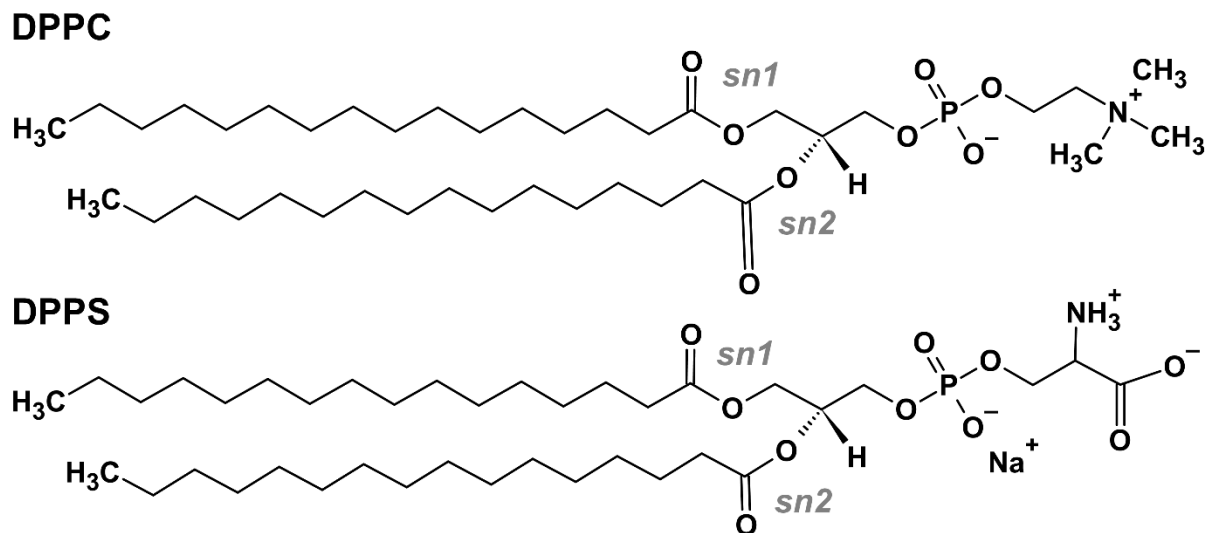


Fig. 1. a) 1,2-dipalmitoyl-*sn*-glycero-3-phosphocholine (DPPC); b) 1,2-dipalmitoyl-*sn*-glycero-3-phosphoserine (DPPS).

2. Experimental

2.1 Chemicals and s/aLUVs preparations

s/aLUVs were prepared from 1,2-dipalmitoyl-*sn*-glycero-3-phosphatidylserine (DPPS), 1,2-dipalmitoyl-*sn*-glycero-3-phosphocholine (DPPC) and 1,2-dipalmitoyl-*sn*-glycero-3-phospho-(1'-*rac*-glycerol) sodium salt (DPPG) that were purchased as white powders from Avanti Polar Lipids ($\geq 99\%$) (DPPG is to be added into sLUVs acceptor in order to prevent/postpone their aggregation [28,30]). Methyl- β -cyclodextrin (m β CD; white powder, $\geq 98\%$), sucrose (C₁₂H₂₂O₁₁; white powder, $\geq 99.5\%$), Tris(hydroxymethyl-d₃)amino-d₂-methane (Tris-d₁₁ or dTris; white powder, 98% atom D) and Tris(hydroxymethyl)aminomethane (hTris; white powder, $\geq 99.8\%$) were purchased from Sigma Aldrich, respectively (note: m β CD, sucrose and hTris are to be dissolved in fresh Milli-Q®). D₂O ($\geq 99.75\%$) and chloroform (CHCl₃; p.a.) were provided from EurIsotop (Saint-Aubin, France) and Carlo Erba (Germany), respectively. HCl and DCl used for pH(D) adjustment of hTris and dTris were purchased from Kemika (p.a.) and Sigma Aldrich (35 wt. % in D₂O, ≥ 99 atom % D), respectively, whereas Pr(NO₃)₃ · 6 H₂O (green crystalline powder, 99.9%) used for ¹H NMR measurements (dissolution of 15 mg of Pr(NO₃)₃ · 6 H₂O in 1.724 ml of D₂O in order to get 20 mM solution) was purchased from Sigma Aldrich.

sLUVs preparation. Separate stock solutions of DPPC, DPPS and DPPG were prepared by dissolving 50 mg of DPPC/DPPS in 5 ml of CHCl₃ and 10 mg of DPPG in 10 ml of CHCl₃ (obtained mass concentrations were $\gamma(\text{DPPC/DPPS}) = 10 \text{ mg ml}^{-1}$ and $\gamma(\text{DPPG}) = 1 \text{ mg ml}^{-1}$). 1 ml of stock solution of DPPC, 1 ml of stock solution of DPPS and 1 ml of stock solution of DPPG (in order to obtain molar fraction of $x(\text{DPPG}) = 5 \%$) were pipetted in flask. CHCl₃ was removed from the flasks on a rotary evaporator to obtain a film that was additionally dried under the Ar stream. In order to prepare the suspension of MLVs, the film was dissolved in 4 ml of Tris-d11 buffer (pD = 7.4) and a mass concentration of lipids was $\gamma(\text{DPPC+DPPS+DPPG}) = 5 \text{ mg ml}^{-1}$. Following three to five cycles of vortexing, heating in a hot bath (~ 70 °C) and cooling in an ice bath (~ 4 °C), MLVs suspension constituted from DPPC+DPPS (+5 % DPPG) was extruded through Avanti® Mini Extruder with holder/heating block at temperature $t \sim 60 \text{ °C}$ through 100 nm pore size of a polycarbonate membrane and with the assistance of 10 mm supporting filters for at least 31 times.

In order to demonstrate that deuterated buffer does not change properties of sLUVs, MLV liposomes of DPPC+DPPS (+ 5% DPPG) in hTris buffer were produced in the same manner as previously described with dTris buffer. Briefly, from the same stock solutions ($\gamma(\text{DPPC/DPPS}) = 10 \text{ mg ml}^{-1}$ and $\gamma(\text{DPPG}) = 1 \text{ mg ml}^{-1}$), 1 ml of stock solutions of DPPC, DPPS and DPPG were pipetted in a flask. After removal of CHCl₃ using rotary evaporator, obtained film was additionally dried under Ar stream and suspended in 4 ml of hTris buffer (the latter was prepared by dissolving of 60 mg of a powder in 20 ml of Milli-Q® so the ionic strength of a buffer prepared was $I(\text{hTris}) = 25 \text{ mM}$, whereas the pH was adjusted to 7.4 by addition of required amount of HCl). The suspension prepared in this way in hTris was treated the same as those obtained in dTris in order to get MLVs and finally sLUVs of DPPC+DPPS (+5 % DPPG) (their calorimetric and selected spectroscopic data are presented in Supporting Information).

aLUVs preparation. m β CD/sucrose aqueous solution of a mass concentration $\gamma = 0.0459 \text{ mg ml}^{-1}$ ($c = 35 \text{ mM}$)/ $\gamma = 0.216 \text{ mg ml}^{-1}$ ($c = 0.632 \text{ M}$) was prepared by dissolving 2.293 g of m β CD powder in 50 ml Milli-Q®/ 10.817 g of sucrose powder in 50 ml of Milli-Q®. Stock solutions of DPPC and DPPS were prepared by dissolving $m(\text{DPPC})/m(\text{DPPS}) = 50 \text{ mg}$ in 5 ml CHCl₃ ($\gamma = 10 \text{ mg ml}^{-1}$) and were further used for the preparation of corresponding films. Specifically, 2 ml of DPPC stock solution was pipetted into a flask and, after removal of CHCl₃ on a rotary evaporator

followed by drying under the Ar stream, the film was suspended in 1 ml of the prepared sucrose solution in order to get to MLVs constituted from DPPC having a concentration $\gamma(\text{DPPC}) = 20 \text{ mg ml}^{-1}$ ($c(\text{DPPC}) = 0.027 \text{ M}$). Separately, 2 ml of a stock solution of DPPS and 982 μl of a stock solution of DPPG were pipetted into a separate flask and a corresponding film was produced after removal of CHCl_3 (using rotary evaporator and drying under Ar stream). DPPS (+ 5% DPPG) film was suspended in 2 ml of dTris buffer (which was prepared by dissolving of 23.13 mg of a powder in 7 ml of D_2O ($I(\text{dTris}) = 25 \text{ mM}$) the pD of which was adjusted to 7.4 by addition of required amount of DCl) so the mass concentration of DPPS (+ 5% DPPG) in a suspension was 10 mg ml^{-1} ($c(\text{DPPS} (+ 5\% \text{ DPPG})) = 0.01 \text{ M}$). Suspensions of DPPC lipids (in the aqueous solution of sucrose) that serve as a donor system [23,28] and those from DPPS + 5% DPPG lipids (in dTris) that stand as an acceptor system [23,28] were exposed to three to five cycles of vortexing, heating in a hot bath ($\sim 70^\circ\text{C}$) and cooling in an ice bath ($\sim 4^\circ\text{C}$) in order to produce MLVs composed from DPPC and DPPS(+ 5% DPPG), respectively. As in the case of sLUVs of DPPC+DPPS (+5 % DPPG) mixture, the suspension of the latter was passed at least 31 times through Avanti® Mini Extruder with holder heating block assembled with a 100 nm pore size of a polycarbonate membrane and with the assistance of 10 mm supporting filters (the temperature of the holder was $t \sim 60^\circ\text{C}$).

aLUVs preparation was followed by 20-fold dilution of 775 μl of DPPC suspension (donor MLVs) by adding 14.7 ml of Milli-Q® followed by centrifugation at 9000g for one hour. After that, supernatant is discarded and a donor precipitate is suspended with 4.43 ml of a stock solution of m β CD so that molar ratio of m β CD:DPPC was 8:1 (note: adding of m β CD solution to the precipitate should be done carefully to minimize the formation of foam). Suspension is transferred to glass vial and left on magnetic stirrer for two hours. In the meantime, Amicon filters (Merck Millipore Ltd.) were rinsed seven times with Milli-Q® for five minutes at 5000g in order to remove glycerol from production. The next step in aLUVs preparation protocol was the incubation of 500 μl of DPPS (+5 % DPPG) (acceptor sLUVs) to the 5.5 ml of m β CD solution containing donor MLVs at $\sim 54^\circ\text{C}$ (temperature only slightly higher than the melting temperature (T_m) of the acceptor LUVs [31]) for 20 minutes with gentle stirring. Mixing is stopped by adding 39.9 ml of Milli-Q® (seven times more than the m β CD–donor–acceptor suspension) and obtained mixture is transferred to a Falcon conical tube and centrifuged at 9000g for one hour. Then, supernatant is carefully pipetted without disturbing the precipitate, divided into two 15-ml Amicon filters and

centrifuged at 5000g for twenty minutes. Filtrate is discarded from Amicon filters and centrifugation is repeated two more times in order to remove residual m β CD and sucrose. 500 μ l of supernatant is pipetted and transferred to Eppendorf tube. The expected final concentration of aLUVs is estimated to be approximately 70 % of initial concentration of DPPS (+5 % DPPG) (acceptor sLUVs).

In order demonstrate the sensitivity of FTIR spectroscopy, as well as to test the reproducibility of the protocol outcome, aLUVs were prepared independently one more time from freshly prepared lipids/cyclodextrin/sucrose stock solutions following the whole procedure described in the last two paragraphs (they are labeled in the continuation of the text as aLUV_{suc}, where index _{uc} stands for unknown concentration). As it will be shown in the text, to low concentration of aLUV_{suc} prevents asymmetry determination using ¹H NMR, but from their FTIR spectra particular asymmetry features can be assessed with certainty.

2.2 Dynamic Light Scattering (DLS): Measurements and data analysis

The size distribution of liposomes was determined with dynamic light scattering measurements using a photon correlation spectrophotometer equipped with a 532 nm (green) laser (Zetasizer Nano ZS, Malvern Instruments, Worcestershire, UK). The average hydrodynamic diameter (d_h) was specified as the value at peak maximum of the volume size distribution. The reported results correspond to the average of six measurements at 25 °C. The data processing was done by the Zetasizer software 802 (Malvern Instruments). The average hydrodynamic diameters values (d_h) of sLUVs (DPPC+DPPS (+5 % DPPG), all at $\gamma = 0.05 \text{ mg ml}^{-1}$) were in the range $250 \text{ nm} \leq d_h \leq 525 \text{ nm}$, whereas analogous values for and aLUVs and aLUV_{suc} (DPPC+DPPS (+5 % DPPG)) were $120 \text{ nm} \leq d_h \leq 315 \text{ nm}$ and $100 \text{ nm} \leq d_h \leq 190 \text{ nm}$, respectively (Fig. S1 in Supporting Information).

2.3 ¹H NMR: Data acquisition and analysis

Proton spectra of s/aLUVs (and aLUV_{suc}) were recorded on Bruker Avance AV600 equipped with 5 mm diameter BBO probe with z-gradient accessory. They were acquired at 30 °C and 65 °C on samples prepared in dTris buffered water using the Bruker standard proton “zg30” pulse sequence (30° flip angle), 2 s delay time, 6009.6 Hz (10 ppm) spectral width, transmitter frequency offset of 2820.61 Hz (4.7 ppm), 32 k time domain and 1024. After collecting the spectra at 30 °C and 65

°C in the absence of Pr³⁺ salt, 2 µl of the 20 mM Pr³⁺/D₂O solution was added directly in the NMR tube and the second pair of ¹H NMR spectra (at 30 °C and 65 °C) was recorded under identical conditions. The procedure was repeated for 4 µl of the 20 mM Pr³⁺/D₂O solution. Obtained NMR spectra were acquired and processed with TopSpin 4.1.3 (Bruker) software package and further analyzed with Spectragryph [32] as follows: in the spectral range 3.27-3.17 ppm the spectra were smoothed (Savitzky-Golay: polynomial of a 3rd degree through 50 points) and baseline corrected. For aLUVs spectrum in the presence of Pr³⁺ the envelope with two maxima at δ = 3.30 ppm and δ = 3.25 ppm was deconvoluted on two Voight's profiles ($R^2=0.998$) and their areas were obtained. Considering the total surface area generated by all choline protons, the fraction of DPPC lipids in particular leaflet was determined [28]. The same procedure could not be applied to the aLUV_{Suc} ¹H NMR spectra due to poor signal intensity.

2.4 Differential scanning calorimetry (DSC): Measurements and data analysis

For the purpose of DSC measurements, microcalorimeter Nano-DSC, TA Instruments (New Castle, USA) was used. Before making the measurements, s/aLUVs and aLUV_{Suc} (DPPC+DPPS (+5 % DPPG)) and a reference solution (dTris buffer) were held for 10 minutes in a degassing station. Thermotropic properties of the samples were examined in the temperature range 10-90 °C at a scanning rate of 1 °C min⁻¹ in two repeated heating-cooling cycles (two heating and two cooling runs). Data analysis, performed using the TA Instruments Nano Analyze software package, started with the subtraction of a heating run curve of s/aLUV_{Suc} from the corresponding heating run curve of dTris and was followed by a baseline correction of obtained curve in selected temperature range (30-65 °C) in which the sample displays melting (DSC curves of sLUVs in hTris are displayed in Supporting Information, Fig. S2).

2.5 FTIR-ATR measurements: Spectra acquisition and data analysis

FTIR ATR spectra of s/aLUVs and aLUV_{Suc} (DPPC+DPPS(+5 % DPPG)) and dTris buffer were collected on Invenio-S Bruker spectrometer, equipped with the photovoltaic LN-MCT detector, using BioATR II unit. The latter is circular with a radius of 2 mm and have upper/lower ATR crystals made of silicon/ZnSe. The ATR unit was continuously purged with N₂ gas connected with external supply and the temperature was kept constant, maintained using a circulating water bath of Huber Ministat 125 temperature controller. All samples were measured at two different

temperatures, 30 °C and 65 °C, with nominal resolution of 2 cm⁻¹ and 256 scans using OPUS 8.5 SPI (20200710) software. FTIR spectra of s/aLUVs (and aLUV_{suc}) were acquired from at least three independent measurements, whereas dTris FTIR spectra were taken once (analogous measurements of sLUVs prepared in hTris are presented in Supporting Information, Fig. S3). Additionally, mβCD and sucrose were dissolved in hTris buffer ($c(\text{m}\beta\text{CD})/c(\text{sucrose})= 0.01 \text{ M}$) and FTIR spectra of their solutions (as well as of hTris) were acquired once at the same temperatures and conditions as the samples' spectra in order to unambiguously confirm their absence from s/aLUVs spectra (the corresponding 2nd derivative spectra are displayed in Supporting Information, Fig. S4.)

The qualitative analysis of FTIR spectra of s/aLUV_{s(uc)} started by subtracting the dTris spectrum from s/aLUV_{s(uc)} spectra collected at the same temperature (Fig. S5. in Supporting Information) followed by smoothing the difference spectra (Savitzky-Golay: polynomial of a 3rd degree through 50 points), taking their second derivative in order to artificially increase spectral resolution [33,34] using Spectragryph software [32], making the baseline correction and performing normalization so that the vibration bands extend in the interval 0-1 (on y-axis). Obtained second derivative spectra were divided in several spectral ranges in order to explore the signatures of particular functional groups of lipids and to find key differences in analogous signatures of sLUVs and aLUV_{s(uc)}. The ranges and associated vibrational signatures were as follows: i) 2980-2820 cm⁻¹ that displays the signatures originated from antisymmetric and symmetric stretching of methylene groups ($\nu_{\text{as}}\text{CH}_2$ and $\nu_{\text{s}}\text{CH}_2$); ii) 1750-1705 cm⁻¹ that displays the signatures originated from the stretching of carbonyl groups ($\nu\text{C=O}$) of *sn*-1 and *sn*-2 chains, both involved in hydrogen bonding (HB) with water molecules and those that are non-hydrogen-bonded (non-HB) (*sn*-1/2 $\nu\text{C=O}_{(\text{non-HB})}$), iii) 1615-1510 cm⁻¹ that displays rather broad signature originated from the antisymmetric stretching of carboxylic groups of DPPS lipids, ($\nu_{\text{as}}\text{COO}^-$), iv) 1510-1390 cm⁻¹ that displays the signature attributed to the scissoring of hydrocarbon chain-constituted methylene groups and the signature of bending of inevitable HOD species (γCH_2 and δHOD); v) 1310-1130 cm⁻¹ that display the signatures of antisymmetric stretching of non-HB and HB phosphate groups ($\nu_{\text{as}}\text{PO}_2^-_{(\text{non-HB})}$) and those of C–O moiety of glycerol backbone, respectively ($\nu_{\text{as}}\text{C–O}$); vi) 1020-910 cm⁻¹ that display variety of signatures originated from (anti)symmetric stretching and bending of choline moieties of DPPC lipids ($\nu_{\text{as}}\text{C–N}$, $\delta_{\text{as}}\text{N–CH}_3$, $\nu_{\text{s}}\text{N–CH}_3$, $\nu_{\text{s}}\text{CNC}$) [35,36].

3. Molecular dynamics simulations

Classical molecular dynamics (MD) was employed for the simulation of symmetric and asymmetric DPPC/DPPS membranes, as well as pure (symmetric) DPPC or DPPS bilayers as control systems. Symmetric (s) DPPC/DPPS bilayers contained equal amounts of both lipids in the upper and lower leaflet. Asymmetric (a) membranes were assembled to contain DPPC molecules in the upper leaflet, and DPPS molecules in the lower leaflet. In asymmetric bilayer simulations, it is necessary to minimize bilayer tension resulting from the mismatch in upper and lower leaflet packing, which is known to cause artifacts in membrane structure and organization [37–41]. From pure (p) DPPC or DPPS bilayer runs, the average area per lipid (APL) for each component in gel and fluid phase was extracted (see section 4.2). Asymmetric bilayer assembly was later done based on those values, by keeping the number of DPPC molecules at 64, and adjusting the number of DPPS molecules in the opposing leaflet so that the total leaflet area was equal. The approach is known as APL matching and is often used in asymmetric bilayer construction [40,42]. Pure DPPC or DPPS bilayers, as well as sDPPC/DPPS thus consisted of 128 (64+64) molecules, while gel phase asymmetric membrane contained 64 DPPC and 67 DPPS lipids, and fluid phase asymmetric membrane contained 64 DPPC and 72 DPPS lipids. The membranes were constructed using the CHARMM-GUI Membrane Builder module [43], and solvated with 50 water molecules per lipid (cca 6400 waters). NaCl was added to neutralize the system and achieve 0.025 M concentration. Thus, all systems contained 2 Cl⁻ ions, while the number of Na⁺ varied (2 in DPPC systems, 130 in DPPS systems, 66 in sDPPC/DPPS, 69 in aDPPC/DPPS in gel phase and 74 for aDPPC/DPPS in fluid phase). Gel phase systems were simulated at 30 °C and fluid phase at 65 °C. Established CHARMM-GUI procedure with gradual reduction of restraints was employed for initial equilibration.

GROMACS 2020.0 software [44] was used for all calculations, using the CHARMM36m force field [45] and the TIP3P water model [46]. The systems first underwent energy minimization by steepest-descent algorithm, followed by 200 ps heating in the NVT ensemble with the V-rescale algorithm, and 200 ns of production in the NpT ensemble (Nosé-Hoover thermostat [47], time constant 1 ps, Parrinello-Rahman barostat [48], target pressure 1 bar, semi-isotropic pressure coupling, time constant 2 ps). The first half of the production run was discarded as equilibration time and only the last 100 ns were analyzed. The time step was 2 fs. Short range Coulomb

interactions and van der Waals interactions were cut off at 12 Å, with the switching function for the latter turned on after 10 Å. Long range Coulomb interactions were handled using particle mesh Ewald (PME) procedure [49]. The bonds involving hydrogen were constrained with LINCS. All simulations were conducted under the three-dimensional periodic boundary conditions. Data analysis was performed with GROMACS modules, Visual Molecular Dynamics (VMD) [50] and Membrbrainy tools [51].

4. Results and Discussion

4.1. Experimental results

The signals corresponding to the protons of the choline moiety in the symmetric (blue curve, Fig. 1a) and asymmetric (red curve, Fig. 2a) LUVs inner and outer leaflet at 30 °C in the absence of Pr³⁺ show a very broad resonance line at 3.27 ppm. The aLUV_{Suc} signal is too weak to be discussed, possibly due to the fact that the majority of lipids are in the gel phase at 30 °C and, therefore, not visible in the NMR spectra. After the addition of Pr³⁺, the signal intensity in both s/aLUVs samples decreases significantly and falls into the baseline for (cyan/orange curve). At 65 °C in sLUVs the resonance line of choline moiety protons at $\delta = 3.27$ ppm is much sharper and of higher intensity, probably due to the majority of lipids existing in the fluid phase (Fig. 2b, lower panel, navy curve). The presence of Pr³⁺ again causes the signal intensity to decrease with the slight shift to higher fields ($\delta = 3.24$ ppm, dark cyan curve). The most interesting result is obtained at 65 °C on aLUVs sample. The resonance line belonging to choline moiety protons in aLUVs at 65 °C at $\delta = 3.26$ ppm (wine curve), as well as that of sLUVs sample, is sharper than those of s/aLUVs obtained at 30 °C because the width of the NMR bands stems from slower/faster rotational diffusion around the longer axis of lipid molecules when they are in the gel/fluid phase [52]. However, after the addition of Pr³⁺ (pink curve), this irregularly shaped broad line splits into two relatively well resolved signals (Fig. 2b, upper panel): those attributed to the inner leaflet choline groups at 3.25 ppm (orange area) and outer leaflet ones at 3.30 ppm (yellow area). Since the area under each signal is proportional to the amount of protonated choline groups present in a given leaflet [28], our data reveal that outer leaflet is populated with ~ 75 % of DPPC lipids, whereas the inner one with ~ 25 %, respectively.

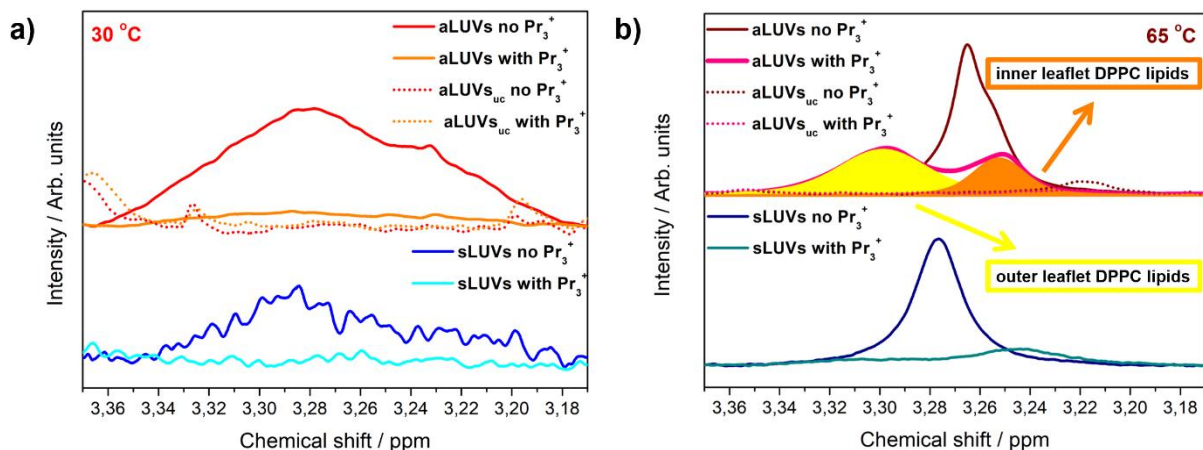


Fig. 2. ^1H NMR spectra of choline protons of s/aLUVs_(uc) in the range 3.37-3.17 ppm acquired at: a) 30 °C in the absence (sLUVs: blue solid curve; aLUVs: red solid curve; aLUVs_(uc): red dotted curve) and the presence of Pr^{3+} (sLUVs: cyan solid curve; aLUVs: orange solid curve; aLUVs_(uc): orange dotted curve); b) 65 °C in the absence (sLUVs: navy solid curve; aLUVs: wine solid curve; aLUVs_(uc): wine dotted curve) and the presence of Pr^{3+} (sLUVs: dark cyan solid curve; aLUVs: pink solid curve; aLUVs_(uc): pink dotted curve). Pink curve (aLUVs at 65 °C) was deconvoluted onto two signals that correspond to DPPC lipids in the outer (yellow) and inner (orange) leaflet, respectively.

Since ^1H NMR spectra confirmed the existence of asymmetric liposomes (aLUVs), we further devoted ourselves to the analysis of s/aLUVs_(uc) thermotropic properties, emphasizing the determination of T_m and the discussion of the melting profile change when the sample is subjected to successive heating and cooling cycles. As expected [20], at the first glance there are considerable qualitative differences between DSC curves obtained in the first (Fig. 3a) and the second (Fig. 3b) heating runs that are attributed to the aLUVs symmetrization upon successive heating/cooling [26]. Melting of sLUVs in the first heating run (Fig. 3a) is presented as a broad curve (blue solid curve) in the temperature range 41-47 °C with a maximum (T_m) at 42.4 °C, whereas in aLUVs the curve is irregularly shaped (red solid curve) with several maxima in range 35-55 °C, and the highest of them is observed at (T_m) at 42.1 °C. aLUVs_(uc), although prepared in the same manner as aLUVs, melt in range 40-60 °C (red dotted curve) and their appearance suggests separate melting of DPPC (42.9 °C) and DPPS (55.6 °C) domains [53,54]. In the second heating run sLUVs (navy solid curve) display the shift of the maximum ($T_m = 44.1$ °C), whereas DSC profile of aLUVs (wine solid curve) becomes less irregular and melts in the range 35-48 °C with $T_m = 42.8$ °C. The melting profile of aLUVs_(uc) (melting in range 41-59 °C) alters as well in terms of merging of DSC curve

maxima (wine dotted curve) into one having maximum at $T_m = 54.6$ °C. Differences in T_m and generally, in melting profiles of sLUVs and aLUVs arise due to, expectedly, asymmetrical distribution of DPPC/DPPS lipids between the leaflets. The difference in T_m between aLUVs and aLUVs_{uc} is attributed to two factors: i) unequal concentrations of DPPC and DPPS in the sample (two independent powders weighing will produce stock solutions that slightly differ in the concentration, whereas the latter further increases by pipetting certain volume from the stock solutions), and ii) unequal DPPC/DPPS distribution between the leaflets. Both of these factors strongly point to general challenges in preparation of aLUVs, especially those concerning reproducibility issues.

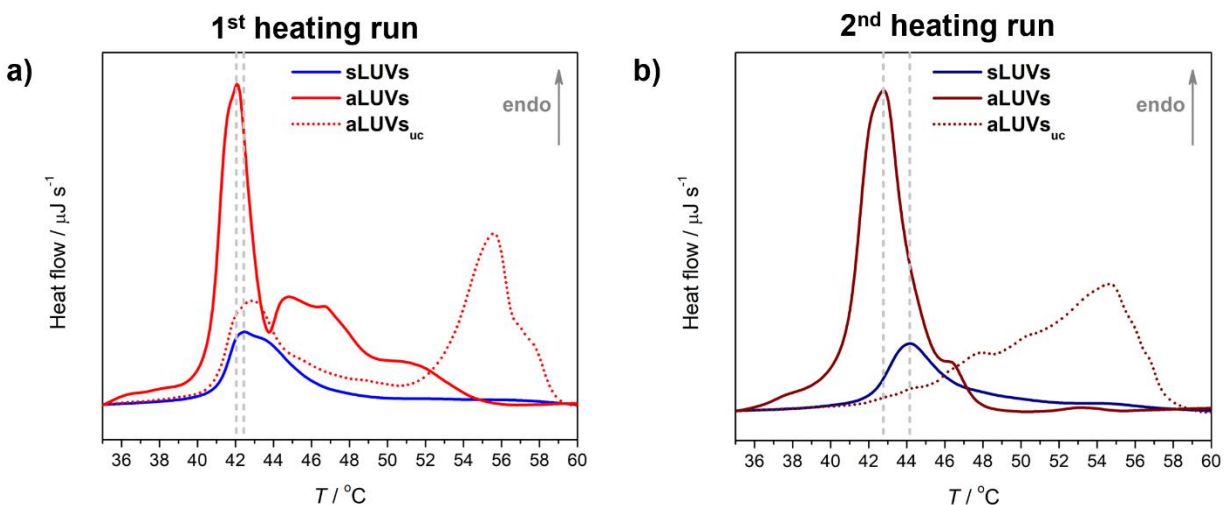


Fig. 3. DSC curves of s/aLUVs_(uc) obtained from: a) 1st heating run: sLUVs as blue solid line, aLUVs as red solid line, aLUVs_(uc) as red dotted line; b) 2nd heating run: sLUVs as navy solid line, aLUVs as olive solid line, aLUVs_(uc) as olive dotted line. T_m of s/aLUVs are highlighted using dashed gray lines.

Characterization of s/aLUVs_(uc) by FTIR spectroscopy (Fig. 4) and determining the asymmetry of aLUVs_(uc) is based on two important assumptions: i) the signatures of certain functional groups should be different enough for sLUVs and aLUVs, and ii) irrespective to the low concentration and/or lower asymmetry degree in aLUVs_{uc}, at least some of their signatures are expected to either resemble the signatures of aLUVs or the superposition the signatures of sLUVs and aLUVs. Should both assumptions be fulfilled, we can be sure that we have found a technique that will be able to detect liposome asymmetry regardless of the amount of asymmetric liposomes, along with their asymmetry degree, that may not be available for characterization by other experimental

techniques. Nevertheless, it has to be emphasized that small amount of DPPG (5 %) do not affect properties of s/aLUVs [30].

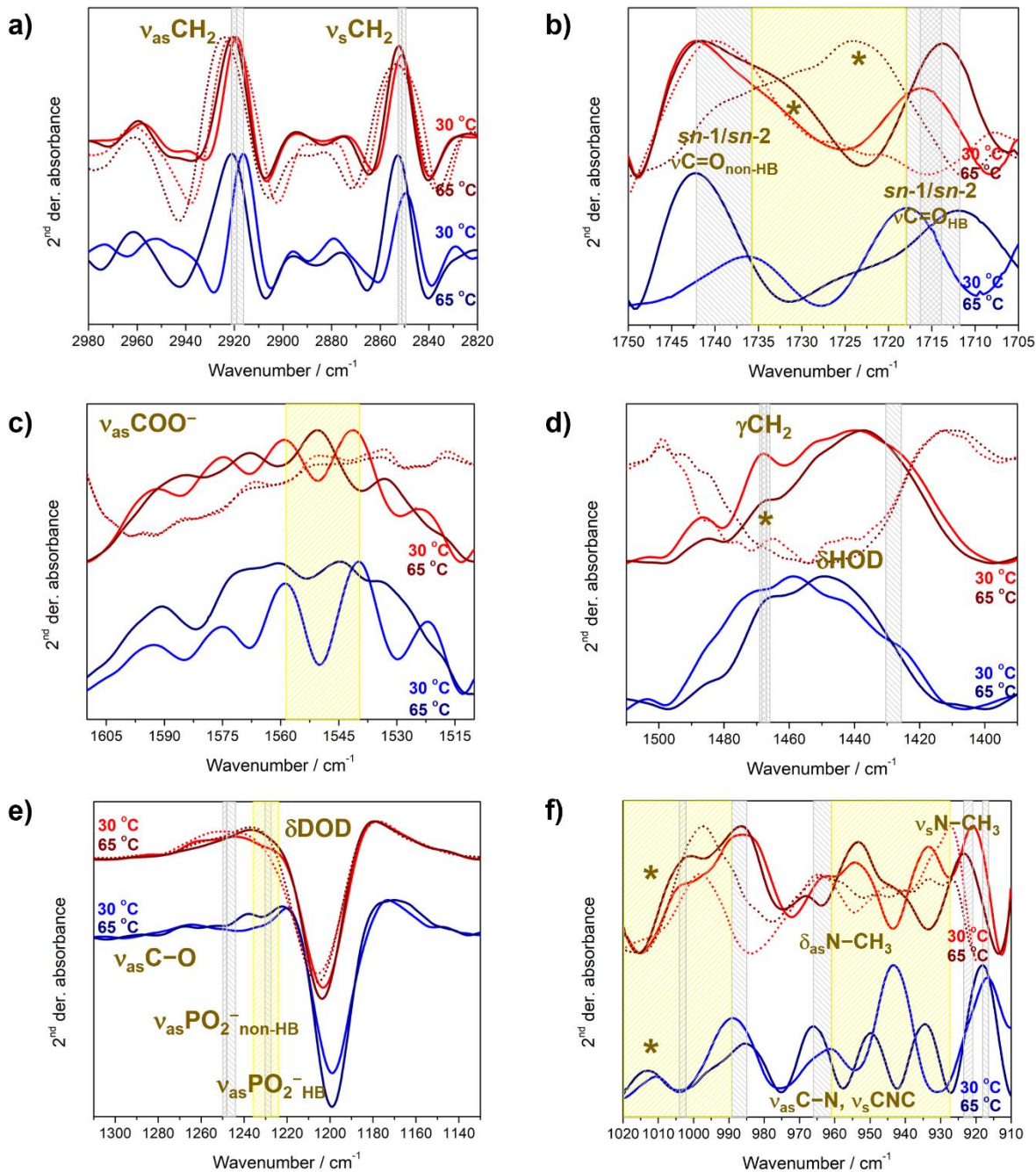


Fig. 4. FTIR spectra of s/aLUVs_(uc) at 30 °C (sLUVs: blue solid curve, aLUVs: red solid curve, aLUVs_(uc): red dotted curve) and 65 °C (sLUVs: navy solid curve, aLUVs: wine solid curve, aLUVs_(uc): wine dotted curve) in following spectral ranges: a) 2980-2820 cm⁻¹ (ν_{as}CH₂ and ν_sCH₂); b) 1750-1705 cm⁻¹ (νC=O); c) 1615-1510 cm⁻¹ (ν_{as}COO⁻); d) 1510-1390 cm⁻¹ (γCH₂ and δHOD); e) 1310-1130 cm⁻¹ (ν_{as}PO₂⁻ and ν_{as}C-O); f) 1020-910 (ν_{as}C-N, δ_{as}N-CH₃, ν_sN-CH₃, ν_sCNC). The phase (temperature)-dependent shifts of particular signatures of s/aLUVs are highlighted with gray rectangles; suspected differences in spectral features between sLUVs and aLUVs are emphasized with yellow rectangles; crucial discriminants between sLUVs and aLUVs_(uc) are additionally labelled with asterisks (*).

In spectral range 2980-2820 cm⁻¹ (Fig. 4a) the signatures originated from ν_{as}CH₂ and ν_sCH₂ display high-wavenumber shift in both s/aLUVs_(uc) as the temperature rises from 30 °C (blue/red solid curves) to 65 °C (navy/wine solid curves); specifically, the signature ν_{as}CH₂ displace roughly from 2918 cm⁻¹ (30 °C) to 2924 cm⁻¹ (65 °C) and ν_sCH₂ from 2848 cm⁻¹ (30 °C) to 2852 cm⁻¹ (65 °C). The features observed at high-frequency side of ν_{as}CH₂ are attributed to the signature of ν_{as}CH₃ and, despite of showing subtle qualitative differences between sLUVs and aLUVs, the vicinity of much stronger features could mask their shape and cannot be addressed as reliable asymmetry-detection probes.

Carbonyl spectral region (νC=O; 1750-1705 cm⁻¹) display signatures of non-HB and HB C=O groups of *sn*-1 and *sn*-2 chain (Fig. 4b) [55–57]. In particular, of *sn*-1/*sn*-2 chains of sLUVs at 30 °C generate generally broad bands that contain contributions of both non-HB and HB C=O groups with maxima at 1736 cm⁻¹/1717 cm⁻¹ (blue solid curves), while at 65 °C (navy solid curves) the corresponding signatures of sLUVs separate and displace to 1743 cm⁻¹/1712 cm⁻¹. In aLUVs at 30 °C (red solid curve) C=O moieties of *sn*-1/*sn*-2 chains produce broad signatures with maxima at 1745 cm⁻¹/1716 cm⁻¹, whereas at 65 °C (wine solid curve) they appear at 1745 cm⁻¹/1712 cm⁻¹. Besides of exhibiting lower displacement than sLUVs, the intrinsically broad signature of aLUVs originated from *sn*-1/*sn*-2 hydrocarbon chain display asymmetry on a low-frequency side (*-labelled), suggesting the increase in the fraction of HB C=O groups of *sn*-1/*sn*-2 hydrocarbon chain. Qualitative differences between signatures of sLUVs and aLUVs might emerge from hydration-related structural changes in the bilayer (when going from sLUVs to aLUVs) such as curvature variations [31]. Interestingly, the signatures of aLUVs_(uc) at 30 °C show certain similarities with corresponding signatures of aLUVs (red dotted curve), whereas at 65 °C (wine

dotted curve) it generates the signature with maximum (*-labelled) in the spectral range in which non-HB C=O group of *sn*-2 hydrocarbon chain absorbs. Although it is not comparable to aLUVs (let's not forget that for now we cannot be sure that aLUV_{Suc} are really asymmetric and that the degree of eventual asymmetry is very likely different from that of aLUVs), one of the possibilities of the appearance of such a derivative spectrum also lies in the structure-dependent change of hydration of glycerol groups, which in any case differs from that of sLUVs.

The broad signature of carboxylic group of DPPS in spectral range 1615-1510 cm⁻¹, regardless of applied smoothing, displays substructures that exhibit the maxima at the same wavenumbers for sLUVs (blue solid curve) and aLUVs (red solid curve) at 30 °C (Fig. 4c). Although there are some changes between sLUVs and aLUVs at 65 °C, emphasizing the maximum at about 1550 cm⁻¹, nothing more can be claimed regarding the utility of this signature as a discriminant between sLUVs and aLUVs. The corresponding signature of aLUV_{Suc} at 30 °C/65 °C (red/wine dotted lines) are by far less intense and stretch over a bit different spectral range because of different amount of H₂O used for their washing during preparation (some steps is impossible to repeat and water traces is impossible to eliminate).

Along with the signature of HOD (δ HOD) that varies between two preparations, spectral region 1510-1390 cm⁻¹ displays the signature of γ CH₂ (Fig. 4d). As one of the most useful signatures in elucidation of hydrocarbon chain lateral packing [31,58], γ CH₂ appears to be useful in discrimination of s/aLUVs signatures. As temperature rises from 30 °C to 65 °C, in sLUVs the signature maximum displaces from 1471 cm⁻¹ (blue solid curve) to 1467 cm⁻¹ (navy solid curve), whereas in aLUVs the corresponding displacement to lower frequencies (red/wine solid curves) is only slightly greater than 1 cm⁻¹. Unfortunately, as this signature is intrinsically not as strong and its intensity decreases as the temperature rises, analogous phenomenon cannot be examined in aLUV_{Suc} since corresponding signature vanishes at 65 °C (red/wine dotted curves). However, the magnitude of the signature shift due to the lipid transition from the gel phase to the fluid phase, suggest that lateral interactions between lipids in sLUVs and aLUVs are different [24].

Spectral region 1310-1130 cm⁻¹ (Fig. 4e) is dominated by the strong absorption minimum of δ DOD signature [35,59], making the signatures of $\nu_{as}PO_2^-$ and $\nu_{as}C-O$ difficult to unambiguously assign [59,60]. Although weak, from the derivative spectra of sLUVs at 30 °C/65 °C (blue/navy

solid curves), minima at $1242\text{ cm}^{-1}/1248\text{ cm}^{-1}$ and $1231\text{ cm}^{-1}/1231\text{ cm}^{-1}$ can be elucidated and are assigned as non-HB and HB phosphate groups [61]. Interestingly, in the spectra of aLUVs at $30\text{ }^{\circ}\text{C}$ (red solid curve) only one minimum is observed at 1231 cm^{-1} , while in aLUVs at $65\text{ }^{\circ}\text{C}$ (wine solid curve) no minimum/maximum is seen. A possible explanation of the observed phenomenon might originate from by far greater extent of HB phosphate groups than non-HB in aLUVs, along with further increase in their fraction by heating which is accompanied by a low-frequency shift under the signature of δDOD . In aLUV_{suc} the corresponding signatures seems to be too weak to be detected.

The last examined spectral region, $1020\text{-}910\text{ cm}^{-1}$ (Fig. 4f) is enriched with variate of signatures originated from choline moiety ($-\text{N}(\text{CH}_3)_3^+$) of DPPC: $\nu_{\text{as}}\text{C-N}$, $\delta_{\text{as}}\text{N-CH}_3$, $\nu_{\text{s}}\text{N-CH}_3$ and $\nu_{\text{s}}\text{CNC}$, which is complex enough when only baseline corrected raw spectral data obtained in transmission are to be examined [35,62,63], not to mention when derivative spectra are taken. However, if we do not insist on a precise assignment but only on the detection of the presence/absence of certain signatures and their displacements, it is immediately noticeable that in sLUVs the signature appears at 1011 cm^{-1} ($30\text{ }^{\circ}\text{C}$)/ 1013 cm^{-1} ($65\text{ }^{\circ}\text{C}$), while in aLUVs (red/wine solid curves) the mentioned signature (*-labelled) is either absent or highly displaced to lower frequencies ($\sim 1000\text{ cm}^{-1}$). According to Fringeli [35], all listed signatures are expected in examined spectral region, but the most likely this particular signature arise from $\nu_{\text{as}}\text{C-N}$ [35]. Additionally, the same signature is absent/displaced from aLUV_{s(suc)} second derivative spectra as well (see red/wine dotted curves), so we could propose that the absence/displacement of this signature implies the existence of unequal distribution of DPPC/DPPS lipids between opposing leaflets. This phenomenon in aLUVs might arise due to different curvature of inner leaflet in aLUVs when compared with sLUVs, especially if the latter contains a larger amount of curvature-favoring DPPS lipids than the outer one; additionally, DPPS lipids are differently hydrated than DPPC ones and, as their number is greater in inner leaflet, they further disturb the hydrogen bond network around DPPC choline moiety (hydration-related issues are presumably reflected also in signatures of $\nu\text{C=O}$, Fig. 4b).

4.2. Molecular dynamics results

MD simulations are useful in illuminating some structural features of lipid bilayers, as well as evaluating their hydration. The commonly analyzed parameters for describing membrane structure

and organization are area per lipid (APL), membrane thickness, acyl chain order and lipid lateral diffusion, while hydration can be evaluated through water density profiles, radial distribution functions (RDFs) and quantifying H-bonds. Here, the symmetric and asymmetric bilayers were analyzed, and also compared to pure DPPC and DPPS membranes as control systems.

APL as a metric of lipid packing is calculated by dividing the surface of the xy plane of the simulation box by the number of lipids in a single leaflet. The values of APL of symmetrical single-lipid systems (Table 1) for gel and fluid phases corresponded well to previous reports [64–68]. APL values are generally lower in gel phase due to closer packing of lipids at lower temperatures, stemming from strong intermolecular interactions. The packing of DPPS is also better compared to DPPC, despite the negative headgroup charge, due to stronger electrostatic interactions and charge dampening of bound Na^+ [67]. As mentioned in the Section 3, pure APL values were employed in generating the asymmetric membrane through area matching.

Table 1. Area per lipid (APL), membrane thickness and lateral diffusion coefficients (D_{lat}) for pure (p), symmetric (s) and asymmetric (a) lipid bilayer systems in gel and fluid phase.

System	APL ^a	Membrane thickness ^b	D_{lat} ^c	
30 °C	pDPPC	0.489 ± 0.005	4.733 ± 0.016	$4.24*10^{-9} \pm 4.88*10^{-10}$
	pDPPS	0.465 ± 0.004	4.453 ± 0.060	$4.86*10^{-9} \pm 5.72*10^{-10}$
	sDPPC	0.476 ± 0.006	4.819 ± 0.016	$4.61*10^{-9} \pm 5.92*10^{-10}$
	sDPPS	0.476 ± 0.006	4.819 ± 0.016	$4.56*10^{-9} \pm 2.07*10^{-10}$
	aDPPC	0.481 ± 0.005	4.660 ± 0.033	$7.92*10^{-9} \pm 1.41*10^{-9}$
	aDPPS	0.459 ± 0.004	4.660 ± 0.033	$4.39*10^{-9} \pm 8.02*10^{-10}$
65 °C	pDPPC	0.634 ± 0.016	4.055 ± 0.018	$1.52*10^{-7} \pm 1.00*10^{-8}$
	pDPPS	0.566 ± 0.014	4.106 ± 0.001	$1.05*10^{-7} \pm 8.00*10^{-9}$
	sDPPC	0.594 ± 0.015	3.843 ± 0.00	$7.46*10^{-8} \pm 9.58*10^{-9}$
	sDPPS	0.594 ± 0.015	3.843 ± 0.00	$6.71*10^{-8} \pm 9.57*10^{-9}$
	aDPPC	0.639 ± 0.015	3.978 ± 0.027	$2.65*10^{-7} \pm 3.20*10^{-8}$
	aDPPS	0.568 ± 0.013	3.978 ± 0.027	$6.11*10^{-8} \pm 6.08*10^{-9}$

^a In nm^2 ; ^b In nm ; ^c In $\text{cm}^2 \text{s}^{-1}$

Construction of an asymmetric membrane in MD poses some unique challenges, mainly due to the fact that different lipids have different optimal packing and APL values, so the same number of

molecules may cover different total area in outer and inner leaflets. In real-world systems, a mismatch in number or total area of outer and inner leaflets would most likely result in bending or lipid flip-flop. In an MD simulation, the nature of the setup (limited size, periodic boundary conditions) forces the bilayer to remain flat and for total area to be equal, and flip-flops are unlikely due to very short time-scales. Since the simulated patch will not bend, and the conditions are artificially keeping it stable, the lipids will adapt by either spreading out or compressing as needed, leading to unrealistic results [37–41]. One of the simplest approaches in optimizing packing to minimize tension is APL matching. The APL value for each lipid, provided from pure bilayer simulations at the exact temperature, is used to match the number of lipids in each leaflet to ensure the total area is equal [42]. The downside of this approach is the ignoring of interleaflet coupling [42], however in this case the APL in asymmetric systems did not deviate significantly from the initial values so it is likely this factor is minimal.

The success of APL matching demonstrates the minimal effect of opposing leaflets on each other's packing. However, when mixed together in the same leaflet, DPPC and DPPS do pack somewhat differently (Table 1), with the APL being in between pure DPPC and DPPS values.

Membrane thickness was estimated as the distance between the average peak positions of lipid phosphorus from number density profiles. Though there are no experimental reports of DPPC-DPPS membrane thickness available, the calculated estimates (Table 1) agree with reports on dipalmitoyl phospholipids [68–70]. Again, pure lipid simulations serve as standards. In gel phase, DPPC bilayer is thicker compared to DPPS, whereas the opposite is the case in fluid phase. In gel, the thickness of aDPPC/DPPS is in between the reference values, while sDPPC/DPPS is thicker than all other bilayers. This would indicate that mixing DPPC and DPPS improves their rigidity and minimizes acyl chain bending, while in asymmetric systems each leaflet is organized as they would be in a pure membrane. On the other hand, in fluid phase both s- and aDPPC/DPPS have lower thickness than both pure systems, meaning chain interdigitation is facilitated. Interleaflet coupling (i.e., the alteration of the properties of one leaflet because of the other [41]) is however less impactful than lipid mixing, so the effect is lesser in aDPPC/DPPS.

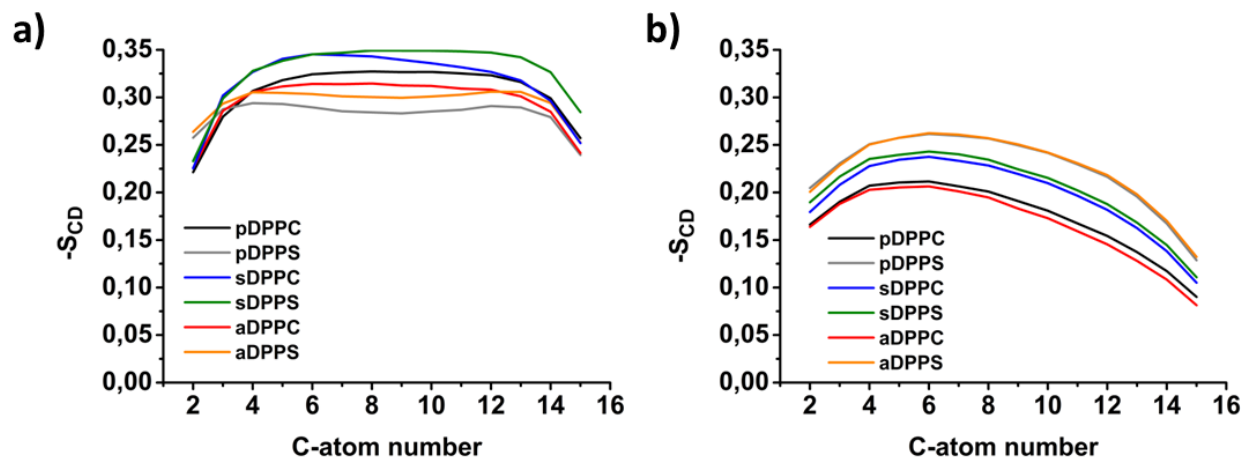


Fig. 5. Acyl chain order parameters (an average of both *sn*-1 and *sn*-2 chains) for pure (p), symmetric (s) and asymmetric (a) lipid bilayer systems at a) 30 °C and b) at 65 °C.

The differing effects in gel or lipid phase are confirmed when acyl chain ordering is analyzed. Order parameters are a measure of the deviation of acyl chains from the rigid straight, vertical position (parallel to membrane normal). Higher values are expected in gel phase where chains are neatly packed and held together strongly with van der Waals interactions, and lower values are an indicator of fluid phase where the chains are bending and interdigitated. Fig. 5 for gel phase shows DPPC is generally more ordered than DPPS, despite DPPS having better packing. This is however in line with membrane thickness data. In aDPPC/DPPS, the ordering of DPPC is decreased, and DPPS increased, towards a medium value, suggesting that there is indeed some degree of interleaflet coupling, since both lipids influence each other to reach a midpoint between their respective ideal organizations. It has been reported that the leaflet with more lipid molecules will become more ordered and vice versa [41]. In contrast, sDPPC/DPPS show a significantly higher degree of order than either of their pure systems, and even the profiles of the curves change. This confirms a synergistic effect of lipid mixing on chain organization that was indicated by membrane thickness. In fluid phase, DPPS is more ordered than DPPC, and asymmetric membrane maintains the same organization for the respective lipids. There appears to be no interleaflet coupling. The effect of lipid mixing in symmetric bilayer still occurs, since DPPS becomes less ordered and DPPC more to reach a medium value. Again, this is consistent with membrane thickness.

The mobility of individual lipids within the membrane is expressed through lateral diffusion coefficient D_{lat} , which is estimated from the mean standard displacement function calculating the

difference between initial and final positions of atom P in relation to time. All estimates (Table 1) were in line with expectations, with mobility being significantly higher in fluid phase where chain interactions are weaker. Though the mobility of pDPPC and pDPPS is roughly the same, in asymmetric membrane DPPC appears more mobile and DPPS less so. Asymmetry has been known to influence lateral diffusion [25]. In gel phase, only the DPPC in aDPPC/DPPS is increased in mobility, while all other values remain consistent. In fluid phase, DPPC in aDPPC/DPPS is again increased in D_{lat} , but every other case is decreased.

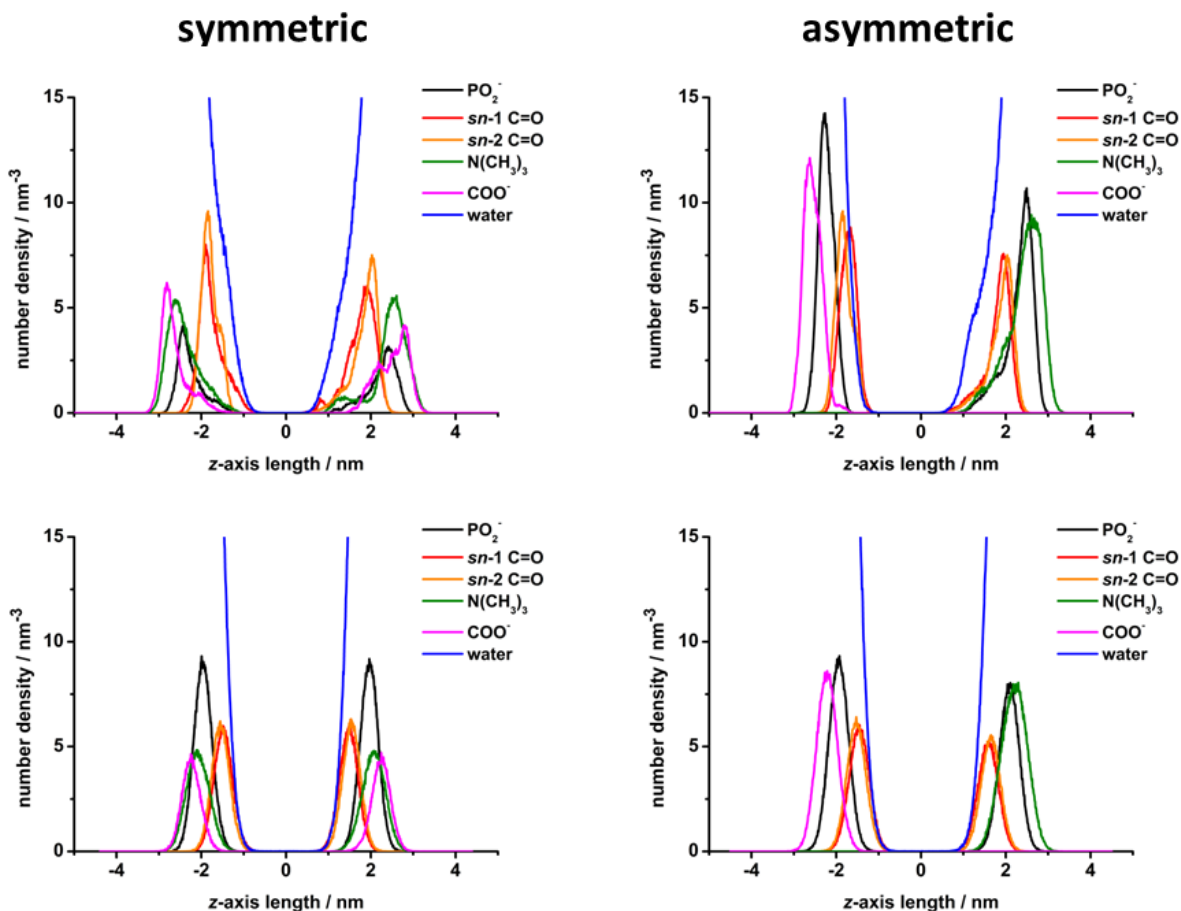


Fig. 6. Number density profiles of symmetric and asymmetric bilayers at 30 °C (top) and 65 °C (bottom).

Number density profiles show the average positioning of certain groups of atoms along the membrane normal. The profiles (Fig. 6 and Fig. S6) show the positions of phosphate groups as delineating the membrane thickness calculation. Choline $N(CH_3)_3$ and COO^- groups are on average positioned closer to the solvent, and $C=O$ groups towards the membrane interior. Usually,

sn-1 C=O are located only slightly closer to center than *sn*-2 C=O. Such distribution is dictated by lipid molecular structure and does not change between systems. However, the profiles also allow for the distribution of water to be examined, which demonstrates membrane hydration and water penetration.

In gel phase, the pure DPPC membranes are by far the most hydrated, and pure DPPS the least. This is in accordance with their APLs as measurements of tightness of headgroup packing. Also, DPPS headgroups are saturated with Na⁺ that likely displaces some water from the surface. On average, water can also penetrate further into the sDPPC/DPPS membrane compared to aDPPC/DPPS, though still falling short of pure DPPC. In the asymmetric membrane, it is seen that the headgroups in each leaflet are packed similarly to their respective pure systems, and that DPPC leaflet is much better hydrated than DPPS. Still, on average the entire system is less hydrated compared to sDPPC/DPPS. In the symmetric membrane, lipid mixing affects the packing somewhat, allowing more water to reach acyl chains. In fluid phase, this effect is almost negligible, meaning temperature and membrane disorder dampen the differences between systems.

Lipid hydration may also be evaluated by analyzing the solvation shell forming around certain groups through RDFs, which provide information on the probability of finding atoms at a certain distance from the reference group. The RDFs of water oxygen were analyzed around lipid functional groups, however they did not depend neither on the lipid type, membrane structure or temperature. Details of this analysis can be found in Supporting information (Section S8).

Table 2. Number of hydrogen bonds established between water and lipid functional groups.

	System	PO ₂ ⁻	<i>sn</i> -1 C=O	<i>sn</i> -2 C=O	COO ⁻
30 °C	pDPPC	490 ± 10	82 ± 6	71 ± 6	/
	pDPPS	363 ± 14	72 ± 5	68 ± 5	589 ± 14
	sDPPC/DPPS	426 ± 11	76 ± 6	72 ± 5	311 ± 10
	aDPPC/DPPS	429 ± 12	72 ± 6	69 ± 6	314 ± 10
65 °C	pDPPC	500 ± 11	98 ± 7	92 ± 7	/
	pDPPS	389 ± 16	90 ± 7	85 ± 7	560 ± 17
	sDPPC/DPPS	445 ± 14	94 ± 7	89 ± 7	297 ± 11
	aDPPC/DPPS	470 ± 14	102 ± 8	94 ± 7	314 ± 13

The H-bond analysis was conducted by defining H-bonds between polar atoms if the distance between the donor and acceptor atoms is ≤ 0.35 nm, and the angle hydrogen-donor-acceptor is $\leq 30^\circ$. Table S1 shows that DPPS in general establishes more H-bonds with water compared to DPPC (~ 11 bonds per lipid molecule vs. ~ 6), which is a reasonable result since DPPS possesses an additional COO^- functional group capable of forming H-bonds. There are generally more H-bonds formed on higher temperatures, likely since lipids are more sparsely packed and it is easier for water to reach the headgroups. In gel phase, the aDPPC/DPPS sees no difference in total H-bonding compared to pure systems, but in sDPPC/DPPS, DPPS binds slightly more waters. In fluid phase, the reverse is true and DPPS in symmetric systems binds slightly less. Though such changes might indicate some influence of lipid mixing on molecular H-bonding, which is not present when DPPC and DPPS are separated into opposite leaflets, the difference is still within method error and therefore too small to be conclusive. Large discrepancy in H-bond count were unlikely considering the simulation setup, since only a very small section of the membrane was observed (~ 128 molecules), and it is possible the effect would be significant on a large scale so that it is visible by FTIR.

Water bonding of particular functional groups was also examined individually (Table 2). Though experimental work indicates potential differences in H-bonding between *sn*-1 and *sn*-2 acyl chains, they are less obvious in simulations. The slight decline in H-bond numbers formed with *sn*-2 C=O is present in all cases, but not statistically significant. Again, the issue might be the limited system size. However, the reason for the effect appearing at all might not be obvious since *sn*-1 C=O is positioned deeper in the membrane and harder to reach by water molecules. It is possible that *sn*-2 C=O bond formation is interrupted by neighboring phosphate that also participates in extensive H-bonding, and it is harder for water molecules to achieve an appropriate angle with C=O. Both C=O and PO_2^- groups form more bonds in DPPC compared to DPPS, even though the entire DPPS molecule is more H-bonded. This is due to the lower degree of headgroup organization in DPPC, making it easier for water to reach those groups. Most additional H-bonds in DPPS stem from the COO^- group which is exposed to the solvent. For the same reason sDPPC/DPPS forms more bonds in gel phase compared to aDPPC/DPPS, since the density profiles showed better water penetration.

Finally, the RDF analysis was employed to examine the interactions and hydration of choline $\text{N}(\text{CH}_3)_3^+$ group, which was of particular interest in FTIR spectra. Fig. S7d in Supporting

Information shows no change in preferred water distribution around $N(CH_3)_3^+$, suggesting the presence or absence of DPPS in the leaflet does not affect solvation shell formation around choline. However, $N(CH_3)_3^+$ does interact with COO^- in sDPPC/DPPS systems, as evidenced from Fig. S8c. Although the preference of choline for PO_2^- group is stronger since there are more phosphates available, its simultaneous tendency towards approaching COO^- could result in differing spectral patterns of sDPPC and aDPPC observed experimentally.

The main takeaway from MD simulations is that between aDPPC/DPPS and sDPPC/DPPS, the differences are predominately structural. Lipid organization and ordering are significantly affected when the two lipids are mixed within the single leaflet, and much less so when leaflets contain only one component. Though interleaflet coupling was expected since it has been proven in aLUVs and aGUVs [25], it was not a major factor here. Most effects seen in aDPPC/DPPS systems could be explained as the averaging of the effects of individual leaflets, which behave similarly to pure systems. Indeed, some reports minimize the occurrence of interleaflet coupling [41,42], especially when the lipid properties are relatively similar. The prevalence of coupling effects will depend on lipid types, composition and temperature [25,39,41]. The temperature effect was certainly in play here, with the synergism of lipid mixing present only in the gel phase. On the other hand, membrane composition had very little impact on headgroup hydration, and the differences that were noticed were only due to the change in packing. These results are similar to a study by Lopez Cascales *et al.* [71] who found that DPPC/DPPS mixed asymmetric membranes had membrane hydration and some structural properties decoupled, but a noted effect on ordering. On the other hand, Porasso *et al.* [72] reported that mixing DPPC and DPPS affects both their organization and hydration. In summary, the study demonstrates the value of MD simulations in discerning some membrane structural properties, especially in conjunction with experiments. However, it also highlights some shortcomings, primarily limited membrane size and inability to evaluate curvature or flip-flop. In addition, it is important to keep in mind that all force fields were extensively parametrized using the data from symmetric membranes, thus there is a gap in knowledge on asymmetric interactions to be filled.

Taking into account all experimental and computational data, we find that the assumptions with which we started the analysis and interpretation of the 2nd derivative of the FTIR spectra are fulfilled and that we have shown that FTIR spectroscopy can truly be used to determine the

asymmetry of liposomes and, additionally, which parts of the lipid molecules are most sensitive to the appearance of asymmetry. Since there are no published structural data on the DPPC/DPPE system, at least as far as we know, this work can serve as a platform on which the preparation process and characterization of the mechanical and structural properties of aLUVs can be obtained. As a first step, one should tackle the reproducibility issue, as well as the inclusion of other buffers in which both lipids can be completely suspended, without the buffer itself preventing the application of other techniques. In this regard, dTris, which was used here primarily for NMR spectra (deuterated solvent) and for good lipid suspension (Tris), actually interferes with the ζ -potential measurement of the s/aLUVs surface due to the interaction of the carboxyl group of the DPPE lipid and the amino group of Tris [73]. The second step concerns the inclusion of other structural and spectroscopic techniques that may provide more detailed molecular picture on the arrangement of lipid molecules at different temperatures (for instance, when one bilayer is in the gel phase and the other in the fluid phase [74]), along with their surface properties that are accessible using temperature-dependent UV-Vis spectroscopy which requires larger volumes of samples [30,31,75,76] that are currently unattainable.

5. Conclusion

In this work s/aLUVs constituted from DPPC(out)/DPPE(in) in dTris were prepared following methyl- β -cyclodextrin-induced lipid exchange technique and their (a)symmetry was confirmed using ^1H NMR technique and was additionally supported with the appearance and changes of DSC curves between the first and the second heating run. FTIR spectra of s/aLUVs were taken and their 2nd derivatives suggest that crucial differences between sLUVs and aLUVs can be unraveled from: i) carbonyl stretching region related with different hydration, ii) the signature of hydrocarbon chain scissoring that reports the change in lipid lateral ordering and iii) with the signature of choline moiety of DPPC lipids that remained in inner leaflet which are sensitive to both hydration and intermolecular interactions with dominantly anionic lipids in their immediate environment. The change in ordering was confirmed by MD simulations, which also indicated the possibility of packing differences affecting hydration. The continuation of this work should include the protocol reproducibility improvement and its adjustment in obtaining larger samples volumes in order to make UV-Vis spectroscopy applicable in aLUVs characterization.

Acknowledgment

This paper was supported by the Croatian Science Foundation, Project No. UIP-2020-02-7669 and by the Croatian Academy of Sciences and Arts. P. M. acknowledges the group led by Dr. Georg Pabst and especially Paulina Piller, M. Sc., from Institute of Molecular Biosciences at University of Graz (Graz, Austria) for a training in the preparation and characterization of asymmetric liposomes, as well as the Head of RBI, Dr. David M. Smith, for providing a grant for this one month-long visit to Graz. The free use (by L. P. and P. M.) of Zetasizer Nano ZS, Malvern (DLS measurements) by Laboratory for biocolloids and surface chemistry (RBI), and of the centrifuge by Laboratory for Protein Biochemistry and Molecular Modelling (RBI) is also deeply appreciated.

Supporting Information

Supporting Information associated with this paper can be found in the online version at <http://>.

References:

- [1] J. Steinkühler, P. Fonda, T. Bhatia, Z. Zhao, F.S.C. Leomil, R. Lipowsky, R. Dimova, Superelasticity of Plasma- and Synthetic Membranes Resulting from Coupling of Membrane Asymmetry, Curvature, and Lipid Sorting, *Adv. Sci.* 8 (2021) 1–9. <https://doi.org/10.1002/advs.202102109>.
- [2] T. Skotland, K. Sagini, K. Sandvig, A. Llorente, An emerging focus on lipids in extracellular vesicles, *Adv. Drug Deliv. Rev.* 159 (2020) 308–321. <https://doi.org/10.1016/j.addr.2020.03.002>.
- [3] D. Degreif, B. Cucu, I. Budin, G. Thiel, A. Bertl, Lipid determinants of endocytosis and exocytosis in budding yeast, *Biochim. Biophys. Acta - Mol. Cell Biol. Lipids.* 1864 (2019) 1005–1016. <https://doi.org/10.1016/j.bbalip.2019.03.007>.
- [4] R. Lipowsky, R. Dimova, Introduction to remodeling of biomembranes, *Soft Matter.* 17 (2021) 214–221. <https://doi.org/10.1039/d0sm90234a>.
- [5] E. Sevcsik, M. Brameshuber, M. Fölser, J. Weghuber, A. Honigmann, G.J. Schütz, GPI-anchored proteins do not reside in ordered domains in the live cell plasma membrane, *Nat. Commun.* 6 (2015) 1–10. <https://doi.org/10.1038/ncomms7969>.
- [6] M. Doktorova, N. Kučerka, J.J. Kinnun, J. Pan, D. Marquardt, H.L. Scott, R.M. Venable,

- R.W. Pastor, S.R. Wassall, J. Katsaras, F.A. Heberle, Molecular Structure of Sphingomyelin in Fluid Phase Bilayers Determined by the Joint Analysis of Small-Angle Neutron and X-ray Scattering Data, *J. Phys. Chem. B.* 124 (2020) 5186–5200. <https://doi.org/10.1021/acs.jpcc.0c03389>.
- [7] M.P.K. Frewein, M. Rumetshofer, G. Pabst, Global small-angle scattering data analysis of inverted hexagonal phases, *J. Appl. Crystallogr.* 52 (2019) 403–414. <https://doi.org/10.1107/S1600576719002760>.
- [8] J.H. Lorent, K.R. Levental, L. Ganesan, G. Rivera-Longworth, E. Sezgin, M. Doktorova, E. Lyman, I. Levental, Plasma membranes are asymmetric in lipid unsaturation, packing and protein shape, *Nat. Chem. Biol.* 16 (2020) 644–652. <https://doi.org/10.1038/s41589-020-0529-6>.
- [9] J.C. Mathai, S. Tristram-Nagle, J.F. Nagle, M.L. Zeidel, Structural determinants of water permeability through the lipid membrane, *J. Gen. Physiol.* 131 (2008) 69–76. <https://doi.org/10.1085/jgp.200709848>.
- [10] R.M. Cordeiro, Molecular Structure and Permeability at the Interface between Phase-Separated Membrane Domains, *J. Phys. Chem. B.* 122 (2018) 6954–6965. <https://doi.org/10.1021/acs.jpcc.8b03406>.
- [11] R.B. Lira, R. Dimova, Fusion assays for model membranes: a critical review, Elsevier Ltd, 2019. <https://doi.org/10.1016/bs.abl.2019.09.003>.
- [12] C. Allolio, A. Magarkar, P. Jurkiewicz, K. Baxová, M. Javanainen, P.E. Mason, R. Šachl, M. Cebecauer, M. Hof, D. Horinek, V. Heinz, R. Rachel, C.M. Ziegler, A. Schröfel, P. Jungwirth, Arginine-rich cell-penetrating peptides induce membrane multilamellarity and subsequently enter via formation of a fusion pore, *Proc. Natl. Acad. Sci. U. S. A.* 115 (2018) 11923–11928. <https://doi.org/10.1073/pnas.1811520115>.
- [13] B. Ding, A. Panahi, J.J. Ho, J.E. Laaser, C.L. Brooks, M.T. Zanni, Z. Chen, Probing site-specific structural information of peptides at model membrane interface in situ, *J. Am. Chem. Soc.* 137 (2015) 10190–10198. <https://doi.org/10.1021/jacs.5b04024>.

- [14] M.T.H. Nguyen, D. Biriukov, C. Tempra, K. Baxova, H. Martinez-Seara, H. Evcı, V. Singh, Š. Radek, M. Hof, P. Jungwirth, M. Javanainen, M. Vazdar, Ionic Strength and Solution Composition Dictate the Adsorption of Cell-Penetrating Peptides onto Phosphatidylcholine Membranes, *Langmuir*. 38 (2022) 11284–11295. <https://doi.org/https://doi.org/10.1021/acs.langmuir.2c01435>.
- [15] M. Krompers, H. Heerklotz, A Guide to Your Desired Lipid-Asymmetric Vesicles, *Membranes (Basel)*. 13 (2023) 267. <https://doi.org/10.3390/membranes13030267>.
- [16] Y.N. Al Badri, C.S. Chaw, A.A. Elkordy, Insights into Asymmetric Liposomes as a Potential Intervention for Drug Delivery Including Pulmonary Nanotherapeutics, *Pharmaceutics*. 15 (2023) 294, 22. <https://doi.org/10.3390/pharmaceutics15010294>.
- [17] C. Drechsler, M. Markones, J.Y. Choi, N. Frieling, S. Fiedler, D.R. Voelker, R. Schubert, H. Heerklotz, Preparation of Asymmetric Liposomes Using a Phosphatidylserine Decarboxylase, *Biophys. J.* 115 (2018) 1509–1517. <https://doi.org/10.1016/j.bpj.2018.08.036>.
- [18] H.Y. Sun, G. Deng, Y.W. Jiang, Y. Zhou, J. Xu, F.G. Wu, Z.W. Yu, Controllable engineering of asymmetric phosphatidylserine-containing lipid vesicles using calcium cations, *Chem. Commun.* 53 (2017) 12762–12765. <https://doi.org/10.1039/c7cc05114j>.
- [19] B. Li, E. London, Preparation and drug entrapment properties of asymmetric liposomes containing cationic and anionic lipids, *Langmuir*. 36 (2020) 12521–12531. <https://doi.org/10.1021/acs.langmuir.0c01968>.
- [20] M. Doktorova, F.A. Heberle, B. Eicher, R.F. Standaert, J. Katsaras, E. London, G. Pabst, D. Marquardt, Preparation of asymmetric phospholipid vesicles for use as cell membrane models, *Nat. Protoc.* 13 (2018) 2086–2101. <https://doi.org/10.1038/s41596-018-0033-6>.
- [21] B. Eicher, F.A. Heberle, D. Marquardt, G.N. Rechberger, J. Katsaras, G. Pabst, Joint small-angle X-ray and neutron scattering data analysis of asymmetric lipid vesicles, *J. Appl. Crystallogr.* 50 (2017) 419–429. <https://doi.org/10.1107/S1600576717000656>.
- [22] S. Pautot, B.J. Frisken, D.A. Weitz, Engineering asymmetric vesicles, *Proc. Natl. Acad. Sci.*

- U. S. A. 100 (2003) 10718–10721. <https://doi.org/10.1073/pnas.1931005100>.
- [23] H.T. Cheng, Megha, E. London, Preparation and properties of asymmetric vesicles that mimic cell membranes. Effect upon lipid raft formation and transmembrane helix orientation, *J. Biol. Chem.* 284 (2009) 6079–6092. <https://doi.org/10.1074/jbc.M806077200>.
- [24] H.T. Cheng, E. London, Preparation and properties of asymmetric large unilamellar vesicles: Interleaflet coupling in asymmetric vesicles is dependent on temperature but not curvature, *Biophys. J.* 100 (2011) 2671–2678. <https://doi.org/10.1016/j.bpj.2011.04.048>.
- [25] F.A. Heberle, D. Marquardt, M. Doktorova, B. Geier, R.F. Standaert, P. Heftberger, B. Kollmitzer, J.D. Nickels, R.A. Dick, G.W. Feigenson, J. Katsaras, E. London, G. Pabst, Subnanometer Structure of an Asymmetric Model Membrane: Interleaflet Coupling Influences Domain Properties, *Langmuir.* 32 (2016) 5195–5200. <https://doi.org/10.1021/acs.langmuir.5b04562>.
- [26] D. Marquardt, F.A. Heberle, T. Miti, B. Eicher, E. London, J. Katsaras, G. Pabst, ¹H NMR Shows Slow Phospholipid Flip-Flop in Gel and Fluid Bilayers, *Langmuir.* 33 (2017) 3731–3741. <https://doi.org/10.1021/acs.langmuir.6b04485>.
- [27] D. Bakarić, D. Petrov, Y. Kunhi Mouvenchery, S. Heissler, C. Oostenbrink, G.E. Schaumann, Ion-induced modification of the sucrose network and its impact on melting of freeze-dried liposomes. DSC and molecular dynamics study, *Chem. Phys. Lipids.* 210 (2018) 38–46.
- [28] M. Doktorova, F.A. Heberle, B. Eicher, R.F. Standaert, J. Katsaras, E. London, G. Pabst, D. Marquardt, Preparation of asymmetric phospholipid vesicles for use as cell membrane models, *Nat. Protoc.* 13 (2018) 2086–2101. <https://doi.org/10.1038/s41596-018-0033-6>.
- [29] O.Y. Selyutina, P.A. Kononova, S.P. Babailov, Complex of praseodymium with lipid as a NMR temperature sensor and probe of liposome states, *New J. Chem.* 44 (2020) 18372–18379. <https://doi.org/10.1039/d0nj03707a>.
- [30] P. Maleš, B. Pem, D. Petrov, D. Domazet Jurašin, D. Bakarić, Deciphering the origin of the

- melting profile of unilamellar phosphatidylcholine liposomes by measuring the turbidity of its suspensions, *Soft Matter*. 18 (2022) 6703–6715. <https://doi.org/https://pubs.rsc.org/en/Content/ArticleLanding/2022/SM/D2SM00878E>.
- [31] L. Pašalić, B. Pem, D. Bakarić, Lamellarity-Driven Differences in Surface Structural Features of DPPS Lipids: Spectroscopic, Calorimetric and Computational Study, *Membranes (Basel)*. 13 (2023) 83, 22.
- [32] F. Menges, “Spectragryph - optical spectroscopy software,” (12.05.2023). <https://www.effemm2.de/spectragryph/>.
- [33] W.F. Maddams, M.J. Southon, III. The effect of band width and band shape on resolution enhancement by derivative spectroscopy, *Spectrochim. Acta Part A Mol. Spectrosc.* 38 (1982) 459–466. [https://doi.org/10.1016/0584-8539\(82\)80022-6](https://doi.org/10.1016/0584-8539(82)80022-6).
- [34] J.J. Max, C. Chapados, Determination of spectroscopic band shapes using second derivatives, part I: Theory, *Appl. Spectrosc.* 69 (2015) 348–362. <https://doi.org/10.1366/13-07446>.
- [35] U.P. Fringeli, H.H. Günthard, Infrared membrane spectroscopy., in: *Mol. Biol. Biochem. Biophys.*, 1981: pp. 270–332. https://doi.org/10.1007/978-3-642-81537-9_6.
- [36] D.G. Cameron, H.L. Casal, H.H. Mantsch, Characterization of the Pretransition in 1, 2-Dipalmitoyl-*sn*-Glycero-3-Phosphocholine by Fourier Transform Infrared Spectroscopy, *Biochemistry*. 19 (1980) 3665–3672. <https://doi.org/10.1021/bi00557a005>.
- [37] H.L. Scott, K.B. Kennison, T.A. Enoki, M. Doktorova, J.J. Kinnun, F.A. Heberle, J. Katsaras, *Model Membrane Systems Used to Study Plasma Membrane Lipid Asymmetry, Symmetry (Basel)*. (2021) 1–21.
- [38] S. Esteban-Martín, H. Jelger Risselada, J. Salgado, S.J. Marrink, Stability of asymmetric lipid bilayers assessed by molecular dynamics simulations, *J. Am. Chem. Soc.* 131 (2009) 15194–15202. <https://doi.org/10.1021/ja904450t>.
- [39] W. Jiang, Y.C. Lin, Y.L. Luo, Mechanical properties of anionic asymmetric bilayers from atomistic simulations, *J. Chem. Phys.* 154 (2021). <https://doi.org/10.1063/5.0048232>.

- [40] J.D. Perlmutter, J.N. Sachs, Interleaflet interaction and asymmetry in phase separated lipid bilayers: Molecular dynamics simulations, *J. Am. Chem. Soc.* 133 (2011) 6563–6577. <https://doi.org/10.1021/ja106626r>.
- [41] M. Blumer, S. Harris, M. Li, L. Martinez, M. Untereiner, P.N. Saeta, T.S. Carpenter, H.I. Ingólfsson, W.F.D. Bennett, Simulations of Asymmetric Membranes Illustrate Cooperative Leaflet Coupling and Lipid Adaptability, *Front. Cell Dev. Biol.* 8 (2020) 1–17. <https://doi.org/10.3389/fcell.2020.00575>.
- [42] S. Park, W. Im, R.W. Pastor, Developing initial conditions for simulations of asymmetric membranes: a practical recommendation, *Biophys. J.* 120 (2021) 5041–5059. <https://doi.org/10.1016/j.bpj.2021.10.009>.
- [43] E.L. Wu, X. Cheng, S. Jo, H. Rui, K.C. Song, E.M. Dávila-Contreras, Y. Qi, J. Lee, V. Monje-Galvan, R.M. Venable, J.B. Klauda, W. Im, CHARMM-GUI Membrane Builder toward realistic biological membrane simulations, *J. Comput. Chem.* 35 (2014) 1997–2004. <https://doi.org/10.1002/jcc.23702>.
- [44] M.J. Abraham, T. Murtola, R. Schulz, S. Páll, J.C. Smith, B. Hess, E. Lindahl, Gromacs: High performance molecular simulations through multi-level parallelism from laptops to supercomputers, *SoftwareX.* 1–2 (2015) 19–25. <https://doi.org/10.1016/j.softx.2015.06.001>.
- [45] J. Huang, S. Rauscher, G. Nawrocki, T. Ran, M. Feig, B.L. De Groot, H. Grubmüller, A.D. MacKerell, CHARMM36m: An improved force field for folded and intrinsically disordered proteins, *Nat. Methods.* 14 (2016) 71–73. <https://doi.org/10.1038/nmeth.4067>.
- [46] W.L. Jorgensen, J. Chandrasekhar, J.D. Madura, R.W. Impey, M.L. Klein, Comparison of simple potential functions for simulating liquid water, *J. Chem. Phys.* 79 (1983) 926–935. <https://doi.org/10.1063/1.445869>.
- [47] S. Nosé, A molecular dynamics method for simulations in the canonical ensemble, *Mol. Phys. An Int. J. Interface Between Chem. Phys.* 52 (1984) 255–268. <http://www.tandfonline.com/loi/tmph20%5Cnhttp://dx.doi.org/10.1080/00268978400101201%5Cnhttp://www.tandfonline.com/>.

- [48] M. Parrinello, A. Rahman, Polymorphic transitions in single crystals: A new molecular dynamics method, *J. Appl. Phys.* 52 (1981) 7182–7190. <https://doi.org/10.1063/1.328693>.
- [49] U. Essmann, L. Perera, M.L. Berkowitz, T. Darden, H. Lee, L.G. Pedersen, A smooth particle mesh Ewald method, *J. Chem. Phys.* 103 (1995) 8577–8593. <https://doi.org/10.1063/1.470117>.
- [50] W. Humphrey, A. Dalke, K. Schulten, VMD: Visual Molecular Dynamics, *J. Mol. Graph.* 14 (1996) 33–38. <https://doi.org/10.1016/j.carbon.2017.07.012>.
- [51] M. Carr, C.E. MacPhee, Membrainy: A “smart”, unified membrane analysis tool, *Source Code Biol. Med.* 10 (2015) 1–10. <https://doi.org/10.1186/s13029-015-0033-7>.
- [52] L. Trahms, An Alternative Interpretation of Nuclear Magnetic Resonance Observations in the Gel State of Lipid Bilayers, *Biophys. J.* 48 (1985) 663–669. [https://doi.org/10.1016/S0006-3495\(85\)83821-2](https://doi.org/10.1016/S0006-3495(85)83821-2).
- [53] Z.D. Schultz, I.M. Pazos, F.K. Mcneil-watson, E.N. Lewis, W. Ira, Implications for Membrane Fusion, *J. Phys. Chem. B.* 113 (2010) 9932–9941. <https://doi.org/10.1021/jp9011944.Magnesium>.
- [54] M.L. Valentine, A.E. Cardenas, R. Elber, C.R. Baiz, Calcium-Lipid Interactions Observed with Isotope-Edited Infrared Spectroscopy, *Biophys. J.* 118 (2020) 2694–2702. <https://doi.org/10.1016/j.bpj.2020.04.013>.
- [55] H.L. Casal, H.H. Mantsch, Polymorphic phase behaviour of phospholipid membranes studied by infrared spectroscopy, *BBA - Rev. Biomembr.* 779 (1984) 381–401. [https://doi.org/10.1016/0304-4157\(84\)90017-0](https://doi.org/10.1016/0304-4157(84)90017-0).
- [56] R.N. Lewis, R.N. McElhaney, W. Pohle, H.H. Mantsch, Components of the carbonyl stretching band in the infrared spectra of hydrated 1,2-diacylglycerolipid bilayers: a reevaluation, *Biophys. J.* 67 (1994) 2367–2375. [https://doi.org/10.1016/S0006-3495\(94\)80723-4](https://doi.org/10.1016/S0006-3495(94)80723-4).
- [57] W. Hübner, A. Blume, Interactions at the lipid-water interface, *Chem. Phys. Lipids.* 96 (1998) 99–123. [https://doi.org/10.1016/S0009-3084\(98\)00083-8](https://doi.org/10.1016/S0009-3084(98)00083-8).

- [58] R.N.A.H. Lewis, R.N. McElhaney, Calorimetric and spectroscopic studies of the thermotropic phase behavior of lipid bilayer model membranes composed of a homologous series of linear saturated phosphatidylserines, *Biophys. J.* 79 (2000) 2043–2055. [https://doi.org/10.1016/S0006-3495\(00\)76452-6](https://doi.org/10.1016/S0006-3495(00)76452-6).
- [59] R.N.A.H. Lewis, R.N. McElhaney, Membrane lipid phase transitions and phase organization studied by Fourier transform infrared spectroscopy, *Biochim. Biophys. Acta - Biomembr.* 1828 (2013) 2347–2358. <https://doi.org/10.1016/j.bbamem.2012.10.018>.
- [60] P.T.T. Wong, H.H. Mantsch, High-pressure infrared spectroscopic evidence of water binding sites in 1,2-diacyl phospholipids, *Chem. Phys. Lipids.* 46 (1988) 213–224. [https://doi.org/10.1016/0009-3084\(88\)90024-2](https://doi.org/10.1016/0009-3084(88)90024-2).
- [61] P. Maleš, Z. Brkljača, I. Crnolatac, D. Bakarić, Application of MCR-ALS with EFA on FT-IR spectra of lipid bilayers in the assessment of phase transition temperatures: Potential for discernment of coupled events, *Colloids Surfaces B Biointerfaces.* 201 (2021) 111645, 8. <https://doi.org/10.1016/j.colsurfb.2021.111645>.
- [62] H.L. Casal, H.H. Mantsch, The thermotropic phase behavior of *N*-methylated dipalmitoylphosphatidylethanolamines, *BBA - Biomembr.* 735 (1983) 387–396. [https://doi.org/10.1016/0005-2736\(83\)90153-0](https://doi.org/10.1016/0005-2736(83)90153-0).
- [63] J. Grdadolnik, D. Hadži, FT infrared and Raman investigation of saccharide-phosphatidylcholine interactions using novel structure probes, *Spectrochim. Acta - Part A Mol. Biomol. Spectrosc.* 54 (1998) 1989–2000. [https://doi.org/10.1016/S1386-1425\(98\)00111-5](https://doi.org/10.1016/S1386-1425(98)00111-5).
- [64] T. Schubert, E. Schneck, M. Tanaka, First order melting transitions of highly ordered dipalmitoyl phosphatidylcholine gel phase membranes in molecular dynamics simulations with atomistic detail, *J. Chem. Phys.* 135 (2011) 055105. <https://doi.org/10.1063/1.3615937>.
- [65] L. Sun, R.A. Böckmann, Membrane phase transition during heating and cooling: molecular insight into reversible melting, *Eur. Biophys. J.* 47 (2018) 151–164. <https://doi.org/10.1007/s00249-017-1237-3>.

- [66] O. Berger, O. Edholm, F. Jähnig, Molecular dynamics simulations of a fluid bilayer of dipalmitoylphosphatidylcholine at full hydration, constant pressure, and constant temperature, *Biophys. J.* 72 (1997) 2002–2013. [https://doi.org/10.1016/S0006-3495\(97\)78845-3](https://doi.org/10.1016/S0006-3495(97)78845-3).
- [67] J.J. López Cascales, J. García de la Torre, S.J. Marrink, H.J.C. Berendsen, Molecular dynamics simulation of a charged biological membrane, *J. Chem. Phys.* 104 (1996) 2713–2720. <https://doi.org/10.1063/1.470992>.
- [68] S.A. Pandit, M.L. Berkowitz, Molecular Dynamics Simulation of Dipalmitoylphosphatidylserine Bilayer with Na⁺ Counterions, *Biophys. J.* 82 (2002) 1818–1827. [https://doi.org/10.1016/S0006-3495\(02\)75532-X](https://doi.org/10.1016/S0006-3495(02)75532-X).
- [69] E. Egberts, S.-J. Marrink, H.C. Berendsen, Molecular dynamics simulation of a phospholipid membrane, *Eur. Biophys. J.* 22 (1994) 423–436. <https://doi.org/10.1007/BF00180163>.
- [70] T. Róg, K. Murzyn, J. Milhaud, M. Karttunen, M. Pasenkiewicz-Gierula, Water Isotope Effect on the Phosphatidylcholine Bilayer Properties: A Molecular Dynamics Simulation Study, *J. Phys. Chem. B.* 113 (2009) 2378–2387. <https://doi.org/10.1021/jp8048235>.
- [71] J.J.L. Cascales, S.D.O. Costa, A. Garro, R.D. Enriz, Mechanical properties of binary DPPC/DPPS bilayers, *RSC Adv.* 2 (2012) 11743. <https://doi.org/10.1039/c2ra21977h>.
- [72] R.D. Porasso, J.J. López Cascales, Study of the effect of Na⁺ and Ca²⁺ ion concentration on the structure of an asymmetric DPPC/DPPC+DPPS lipid bilayer by molecular dynamics simulation, *Colloids Surfaces B Biointerfaces.* 73 (2009) 42–50. <https://doi.org/10.1016/j.colsurfb.2009.04.028>.
- [73] W. Inam, R. Bhadane, R.N. Akpolat, R.A. Taiseer, S.K. Filippov, O.M.H. Salo-Ahen, J.M. Rosenholm, H. Zhang, Interactions between polymeric nanoparticles and different buffers as investigated by zeta potential measurements and molecular dynamics simulations, *View.* 3 (2022) 1–20. <https://doi.org/10.1002/VIW.20210009>.
- [74] B. Eicher, D. Marquardt, F.A. Heberle, I. Letofsky-Papst, G.N. Rechberger, M.S. Appavou,

- J. Katsaras, G. Pabst, Intrinsic Curvature-Mediated Transbilayer Coupling in Asymmetric Lipid Vesicles, *Biophys. J.* 114 (2018) 146–157. <https://doi.org/10.1016/j.bpj.2017.11.009>.
- [75] P. Maleš, Z. Brkljača, D. Domazet Jurašin, D. Bakarić, New Spirit of an Old Technique: Characterization of Lipid Phase Transitions via UV/Vis Spectroscopy, *Spectrochim. Acta Part A Mol. Biomol. Spectrosc.* 272 (2022) 121013, 7. <https://doi.org/10.1016/j.saa.2022.121013>.
- [76] P. Maleš, M. Butumović, I. Erceg, Z. Brkljača, D. Bakarić, Influence of DPPE Surface Undulations on Melting Temperature Determination: UV/Vis spectroscopic and MD study, *Biochim. Biophysica Acta Biomembr.* 1865 (2023) 184072, 9.